N O T I C E

THIS DOCUMENT HAS BEEN REPRODUCED FROM MICROFICHE. ALTHOUGH IT IS RECOGNIZED THAT CERTAIN PORTIONS ARE ILLEGIBLE, IT IS BEING RELEASED IN THE INTEREST OF MAKING AVAILABLE AS MUCH INFORMATION AS POSSIBLE

OLD DOMINION UNIVERSITY RESEARCH FOUNDATION

DEPARTMENT OF MECHANICAL ENGINEERING AND MECHANICS
SCHOOL OF ENGINEERING
OLD DOMINION UNIVERSITY
NORFOLK, VIRGINIA

EXPERIMENTAL STUDY OF FLOW DUE TO AN ISOLATED SUCTION HOLE AND A PARTIALLY PLUGGED SUCTION SLOT

By

Stephen P. Wilkinson

Principal Investigator: G.L. Goglia

Final Report
For the period February 1, 1978 - January 31, 1980

Prepared for the
National Aeronautics and Space Administration
Langley Research Center
Hampton, Virginia

Under NSG-
Research Grant 1491
Dennis M. Bushnell, Technical Monitor
High-Speed Aerodynamics Division

February 1980

DEPARTMENT OF MECHANICAL ENGINEERING AND MECHANICS
SCHOOL OF ENGINEERING
OLD DOMINION UNIVERSITY
NORFOLK, VIRGINIA

EXPERIMENTAL STUDY OF FLOW DUE TO AN ISOLATED SUCTION HOLE AND A PARTIALLY PLUGGED SUCTION SLOT

By

Stephen P. Wilkinson

Principal Investigator: G.L. Goglia

Final Report
For the period February 1, 1978 - January 31, 1980

Prepared for the
National Aeronautics and Space Administration
Langley Research Center
Hampton, Virginia 23665

Under
Research Grant 1491
Dennis M. Bushnell, Technical Monitor
High-Speed Aerodynamics Division

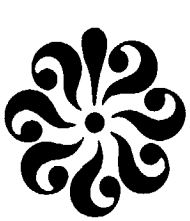

Submitted by the
Old Dominion University Research Foundation
P.O. Box 6369
Norfolk, Virginia 23508

February 1980

TABLE OF CONTENTS

LIST OF FIGURES

LIST OF FIGURES

EXPERIMENTAL STUDY OF FLOW DUE TO AN ISOLATED SUCTION HOLE AND A PARTIALLY PLUGGED SUCTION SLOT

By

Stephen P. Wilkinson[1]

SUMMARY

Details for construction of a model of a partially plugged, laminar flow control (LFC), suction slot and an isolated hole are presented. The experimental wind-tunnel facility and instrumentation is described. Preliminary boundary-layer velocity profiles (without suction model) are presented and shown to be in good agreement with the Blasius laminar profile. Recommendations for the completion of the study are made. In the appendix, an experimental program for study of transition on a rotating disk is described along with preliminary disturbance amplification rate data.

INTRODUCTION

The object of the current research was to obtain quantitative, three-dimensional mean flow and fluctuation (u', v', w') measurements as well as flow visualization data for a single isolated suction opening and a partially plugged suction slot in a laminar boundary layer in air. The rationale behind the research was to provide experimental comparsion/calibration data for use with theoretical efforts to optimize wall suction parameters for laminar flow control (LFC) applications. A required relocation, however, of the NASA/Langley Research Center (LaRC) 15-Inch Low Turbulence Tunnel (in which the experiments were to be conducted) and a change in experimental priorities necessitated that the incomplete program be redirected. The new area of research, also directly related to LFC technology, was to conduct a hot wire anemometer study of the

[1] Research Instructor, Old Dominion University Research Foundation, P.O. Box 6369, Norfolk, Virginia, 23508.

transition process in the three-dimensional boundary layer on a flat disk rotating in still air. The crossflow (radial) velocity profile on a flat rotating disk is similar to that on a swept airfoil and, therefore, presents an experimental alternative for study of the crossflow instability.

Reported herein is a description of the isolated hole/partially plugged slot experiments as far as they were carried out—i.e., through the facility construction and calibration stages. No data for the suction models is available at this time. Recommendations for completion of the research are made. Also, in the Appendix, a progress report on the rotating disk experiments is presented along with preliminary boundary-layer disturbance growth rate data and recommendations for future study.

NOMENCLATURE

c_q	suction coefficient = $\frac{(\rho v)_\infty}{(\rho U)_\infty}$
E	hot wire anemometer output
E_o	hot wire anemometer output at zero velocity
H	shape factor = δ^*/θ
k_s	roughness height
L/D	hot wire length to diameter ratio
P	static pressure
P_x	static pressure at streamwise location X
Q	suction volume flow rate
R	radius
Re	Reynolds number
Re_s	$\frac{v_o s}{\nu}$
Re_x	$U_\infty x/\nu$
Re_θ	$U_\infty \theta/\nu$
R_h	parameter defined by equation (1)
R_H/R_C	ratio of hot wire operating resistance to resistance at ambient temperature

s	slot width
U	velocity
U_∞	stream velocity
u'	streamwise or tangential velocity fluctuation
v'	vertical velocity fluctuation
w'	spanwise velocity fluctuation
$\frac{du}{dy}\Big\|_w$	velocity gradient at wall
v_o	suction velocity
x	streamwise coordinate
y	vertical coordinate
z	spanwise coordinate
δ	boundary-layer thickness
δ^*	displacement thickness
θ	momentum thickness
ρ	density
ν	kinematic viscosity = μ/ρ
ω	rotation rate (rad/sec)
μ	absolute viscosity

SUCTION EXPERIMENTS—BACKROUND

Application of suction to a laminar boundary layer has the simultaneous effects of both stabilizing the flow and reducing drag, with the latter being due to the prevention of transition to turbulence. The economic impact of the drag reduction is the primary reason for the current interest in LFC research. An extensive review and bibliography of LFC through 1979 is provided in reference 1.

Suction surfaces may be broadly characterized as to whether the inflow is two- or three-dimensional (ref. 2). The two-dimensional category

includes spanwise slots, porous strips, and an ideally wholly porous surface. The three-dimensional case consists of any array of discrete perforations. As the size and spacing of the perforations is reduced, the two-dimensional case is approached.

Optimization of LFC suction rate and distribution requirements relies on a combination of analytical, numerical, and empirical methods. Basically, three steps are involved (ref. 1): (1) calculation of the mean (viscous) flow development; (2) calculation of the unsteady or stability characteristics of these profiles, and (3) relation of the stability theory to the transition location. The aim of the current research was to provide experimental data related to the first two steps for two suction configurations of particular interest—a single isolated hole and a partially plugged slot.

Direct numerical solution techniques are generally available for many boundary-layer flow problems, but as yet none can successfully deal with the complex three-dimensional flow field created by a discrete suction opening. LFC research has shown that very narrow spanwise slots or arrays of small discrete hole are the preferable methods for application of suction as opposed to wide slots or porous materials. Due to the small width of the slots (approximately 0.1 mm), blockage by foreign matter (dust, insects, etc.) must be anticipated. This blockage creates a discrete three-dimensional disturbance in the flow field. Therefore, the detailed mean flow and oscillatory flow characteristics due to the partially plugged slot are of interest as well as those due to an isolated suction hole. Arrays of holes or slot blockages can exhibit flow phenomena dependent upon array geometry. The principle phenomena include standing vortex bridges between holes and shedding of horseshoe vorticies (ref. 3). The effect of array geometry on transition has been experimentally investigated by work at Northrop under Pfenninger (for example, ref. 4). The detailed velocity mapping of such flow fields, however, represents a formidable experimental task and should be attempted only following successful completion of the current research.

MODEL DESIGN CONSIDERATIONS

The geometry and flow parameters for LFC slot suction have been determined experimentally. Pfenninger (ref. 5) notes that slot wake oscillations in the slot exit of the small spanwise plenum chambers underneath the slots at flow Reynolds number $R_s > 100$ induce flow fluctuations at the slot inlet which lead to premature transition. Therefore, the slot designed for the experimental study should correspond to $R_s < 100$. Futhermore, according to reference 6, the slot width should be approximately equal to the sucked height of the boundary layer. The sucked height is that height at which the mass flow in the boundary-layer flow below that point is equal to the mass flow going into the slot. Another requirement is that no spanwise pressure gradient should exist along the slot which would cause a three-dimensional inflow (ref. 1). In reference 7, it is pointed out that relatively shallow plenum chambers are preferable to deeper ones for the prevention of suction flow oscillations.

The experiments will be carried out in air in a Blasius laminar boundary layer. In order to make use of hot wire probes capable of resolving three velocity components and in order to make best use of smoke-flow visualization methods, a relatively thick boundary layer (low stream velocity) is required.

The above considerations are sufficient to determine a slot suction system consistent with current LFC practice. A preliminary sketch of a slot meeting the necessary criteria is shown in figure 1, along with appropriate flow parameters. The high-density porous plug shown in the plenum chamber is used to minimize spanwise pressure variation within the plenum chamber. Mean flow measurements for the unblocked slot will be made and compared to data in the literature (ref. 8) to establish baseline data. Partially blocking the slot with a square element will provide the model for detailed three-dimensional investigation. A square blockage element was chosen to simulate the most probable sized foreign element which would become lodged in the slot, i.e., a particle whose size is on the order of the slot width. Both flush and nonflush blockage elements will be considered.

Re_x AT SLOT = 120,000

x = 0.6 mm

δ = 8.7 mm

$c_q = \frac{v_o}{U_\infty} = 0.1$

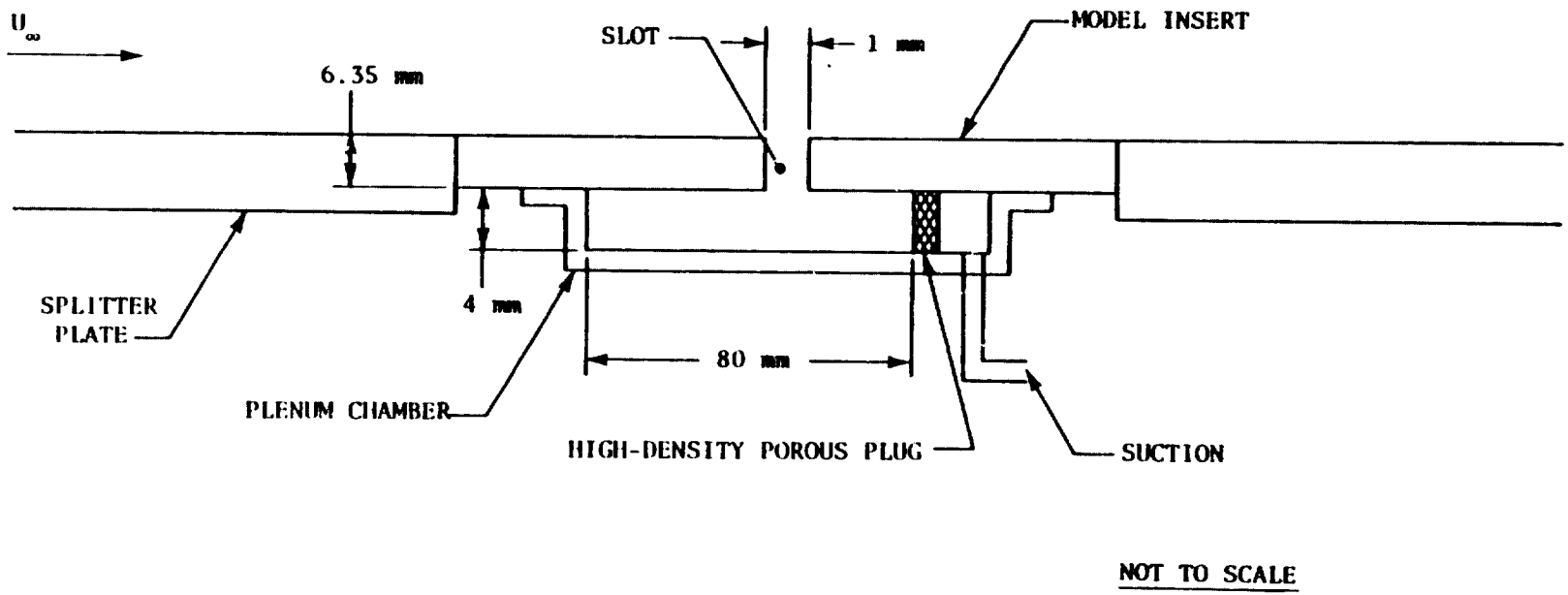

Figure 1. Proposed two-dimensional slot model for suction blockage experiment.

Reference 3 describes critical suction parameters for a single suction hole and a row of holes. The basic criterion for a single hole is the parameter R_h, defined by:

$$R_h = \frac{1}{\nu} Q^{2/3} \left(\frac{du}{dy}\right)_w^{1/3} \tag{1}$$

which should be less than 950 to avoid premature transition. Using the same boundary layer as described in figure 1, a 2.54-mm diameter circular hole with a mean suction velocity of 14.6 m/s will meet the above criterion and provide adequate size for detailed hot wire study.

EXPERIMENTAL APPARATUS

Wind Tunnel

The wind tunnel in which the experiments are to be performed is an open-loop unit, as shown in figure 2. Stable, very low speeds (approximately 3 m/s) are obtainable by venting the tunnel downstream of the test section. Free-stream turbulence control is provided by an inlet honeycomb, a series of screens, and a 20:1 nozzle area contraction ratio. Actual free-stream turbulence intensity has not yet been measured. The tunnel contains a unique muffler-diffuser downstream of the test section. The muffler is basically a box filled with glass fiber with an expanding diffuser through it. The diffuser is divided into four equal channels by a cruciform wedge which is filled with glass fiber and faced with fiberglass cloth. The purpose of the wedge is to attenuate high-frequency noise generated downstream.

The test section is shown in figure 3. It is constructed from 1.27-cm thick Plexiglas to facilitate flow visualization studies. The upper and lower walls are adjustable to provide for maintenance of a zero free-stream pressure gradient. A horizontal 1.27-cm thick Plexiglas splitter plate is mounted on the centerline of the test section. The leading edge is elliptical in shape with a major axis of 30.48 cm and a minor axis of 0.635 cm. It was machined from aluminum and buffed to a gloss finish. The upper channel of the test section is designated as the test area while the lower

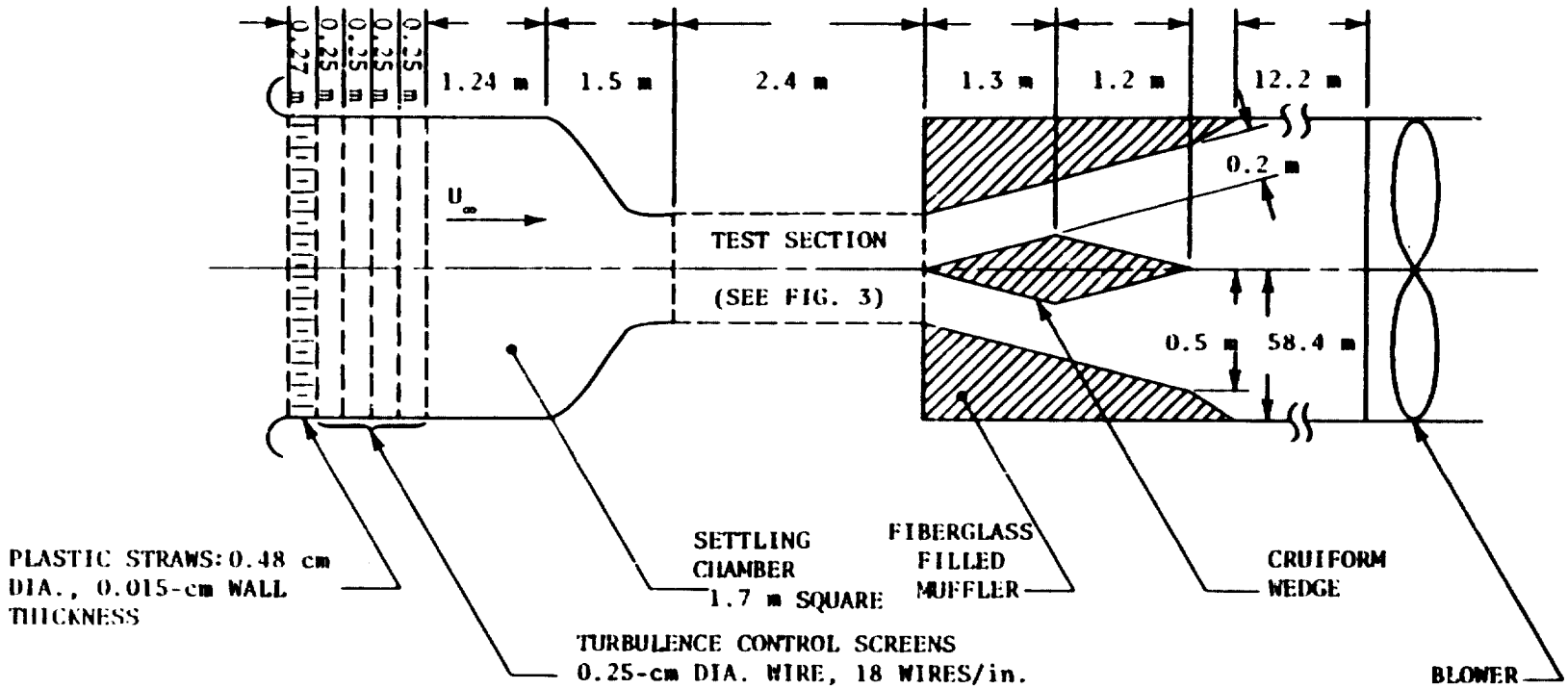

Figure 2. Wind tunnel (side view).

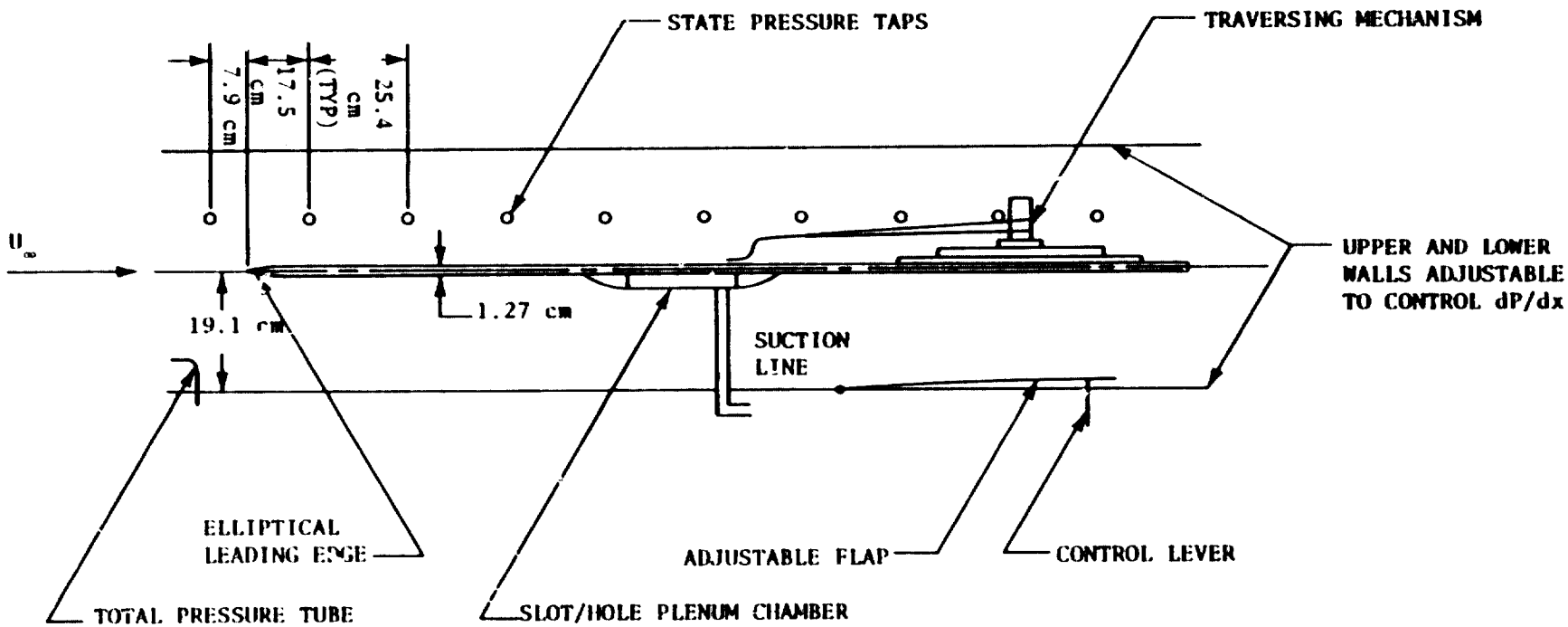

Figure 3. Test section (side view).

chamber contains the suction plenum chamber and miscellaneous cables, tubes, etc. associated with the experiments. The test model will be located approximately 0.7 m from the leading edge.

Instrumentation

Traversing mechanism.—A three-axis traversing mechanism with an X, Y, Z range of 38, 25, and 6 cm respectively is placed on the splitter plate. The entire mechanism can be moved fore and aft as required. A 91-cm sting is mounted on the vertical (Z) axis to position the probe well out of the disturbance region of the traversing mechanism. The traversing apparatus causes approximately 10 percent area blockage in the upper channel of the test section. To compensate for this, an adjustable flap is provided in the lower channel to balance the flow in the upper and lower channels. Each axis of the mechanism is motor driven under computer control and is equipped with an optical shaft encoder to provide positional resolution of ±0.013 mm.

Total pressure tube, static pressure taps and transducer.—A total pressure tube is mounted 7.5 cm from the lower wall of the test section, 2.5-cm upstream of the leading edge. Static pressure orifices are provided at 25.4-cm intervals along the side wall of the upper channel. Stream velocity and streamwise pressure gradient are calculated from readings from a Validyne model DP103 pressure gauge whose full-scale pressure range is ±69 Pa. The gauge has a full-scale calibration accuracy of ±0.025 mm H_2O and a linearity of better than ±0.5 percent full scale.

Hot wire anemometer system.—For the initial boundary-layer mean velocity surveys (no suction model), a single-channel, constant temperature, hot wire anemometer was used. A miniature boundary-layer probe (TSI model 1261) with a 1-mm long, 0.0036-mm diameter tungsten wire was employed. For later three-dimensional measurements with the models, a three-dimensional probe will be constructed.

Hot wire calibration system.—The free-stream velocity for these experiments is approximately 3 m/s. The pressure instrumentation used

for measurement of the free-stream velocity does not have sufficient accuracy at the very low boundary-layer total pressures; therefore, the hot wire cannot be calibrated in the test section free stream. To overcome this difficulty, an alternate calibration technique was developed. It is based on moving the probe through still air by means of a pendulum and photoelectrically measuring the velocity of the pendulum while simultaneously measuring the anemometer output. The hot wire was mounted at a variable point along the pendulum with the wire horizontal and oriented perpendicular to the tangential motion of the pendulum (see fig. 4). The pendulum was released into still air from a variable initial angle. As the pendulum passed its lowest point, the speed of the pendulum was clocked with a photoelectric timer. The timer consisted of a focused light beam, a phototransistor receptor circuit, and a 5.08-cm wide timing plate attached to the pendulum. The light beam was brought to an approximate point focus 2.042 m from the center of rotation in the path of the timing plate. As the plate passed through the beam, the receptor circuit output a pulse whose width was proportional to the speed of the pendulum at the timing plate. The leading edge of this pulse was used to trigger a digital voltmeter to record the anemometer output. Figure 5 shows the ratio of the tangential velocity U at any point along the pendulum to the maximum velocity U_{max} of that point ($\theta = 0$) as a function of θ for several values of θ_o. The curves were calculated assuming an ideal simple pendulum. The timing plate occupied a total angle of approximately 1.5 degrees. From the graph, it is seen that for all $\theta_o > 10$ degrees, the velocity as determined with the timing plate will have an uncertainty of less than 0.5 percent ($U/U_{max} > 0.995$). The integration period of the digital voltmeter was 0.05 sec, and the width of the timing pulse was always greater than that for all $\theta_o > 10$ degrees. By varying θ_o and the position of the probe along the pendulum, an accurate, low-velocity calibration of the probe could be obtained. A representative calibration curve is shown in figure 6.

A second order, least squares fit of the data in the form $E^2 - (0.9E_o)^2$ and $\sqrt{U}$ results in an equation:

$$E^2 = A + B\sqrt{U} + C\,U \qquad (2)$$

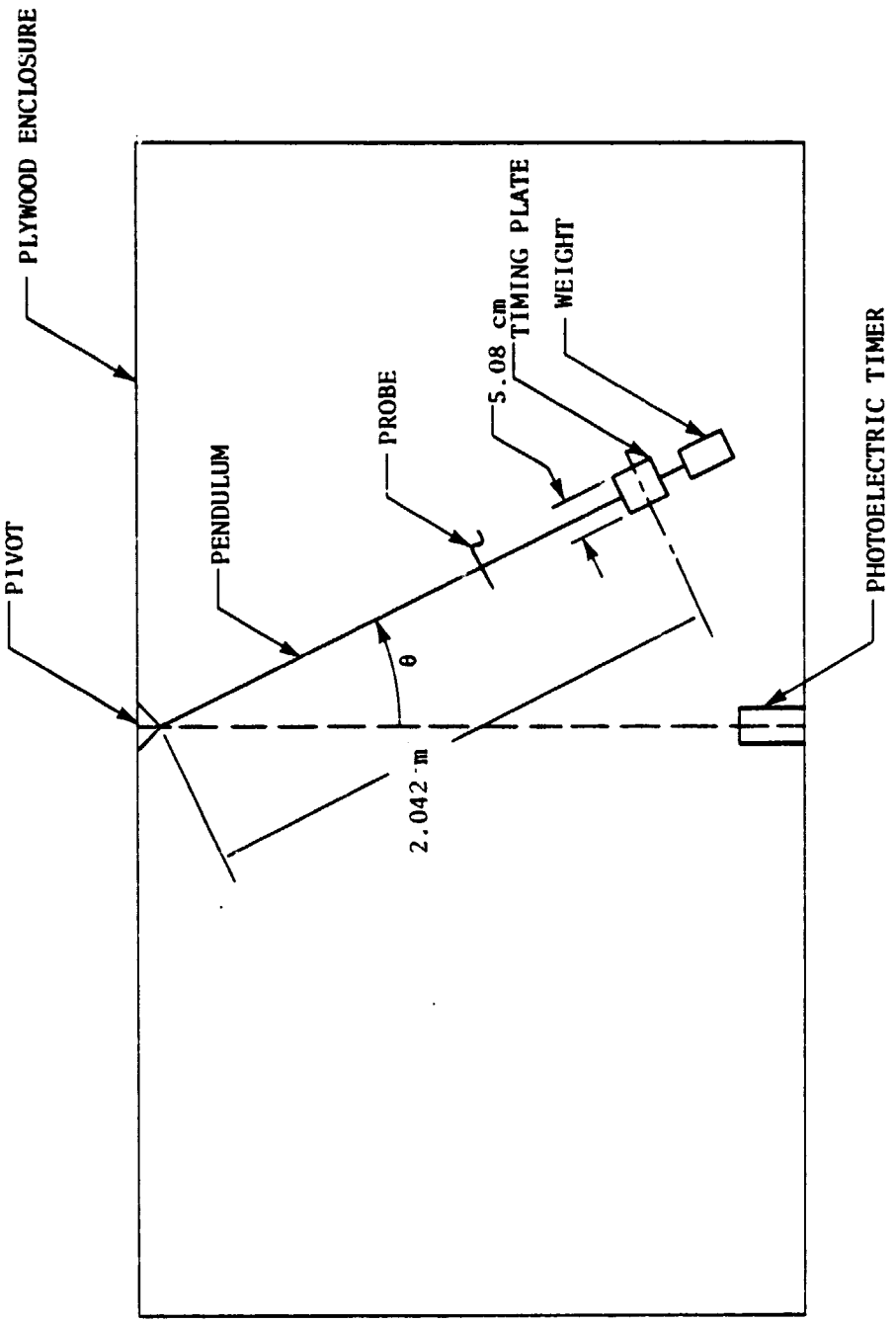

Figure 4. Hot wire calibration apparatus.

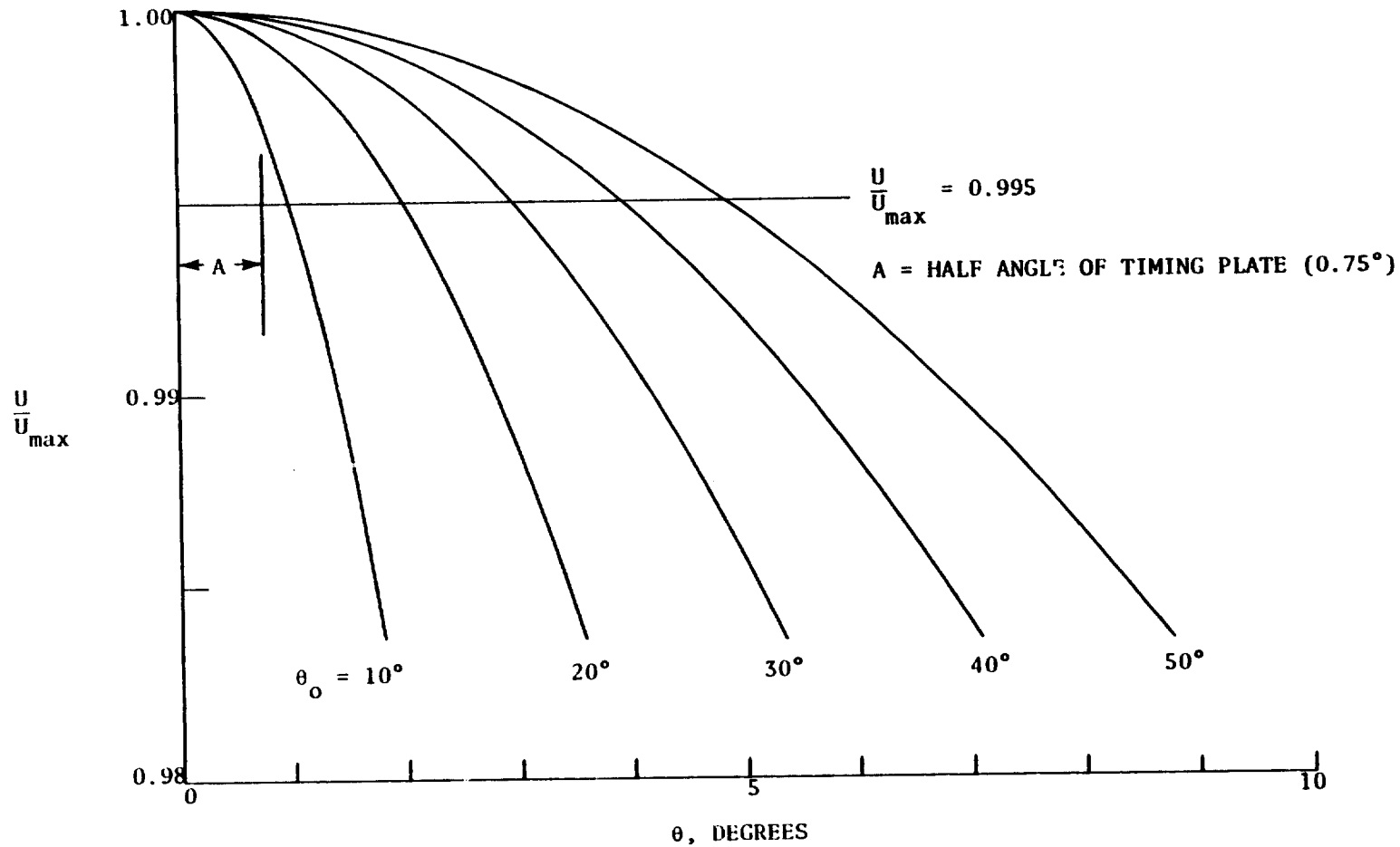

Figure 5. Variation of pendulum velocity with angle.

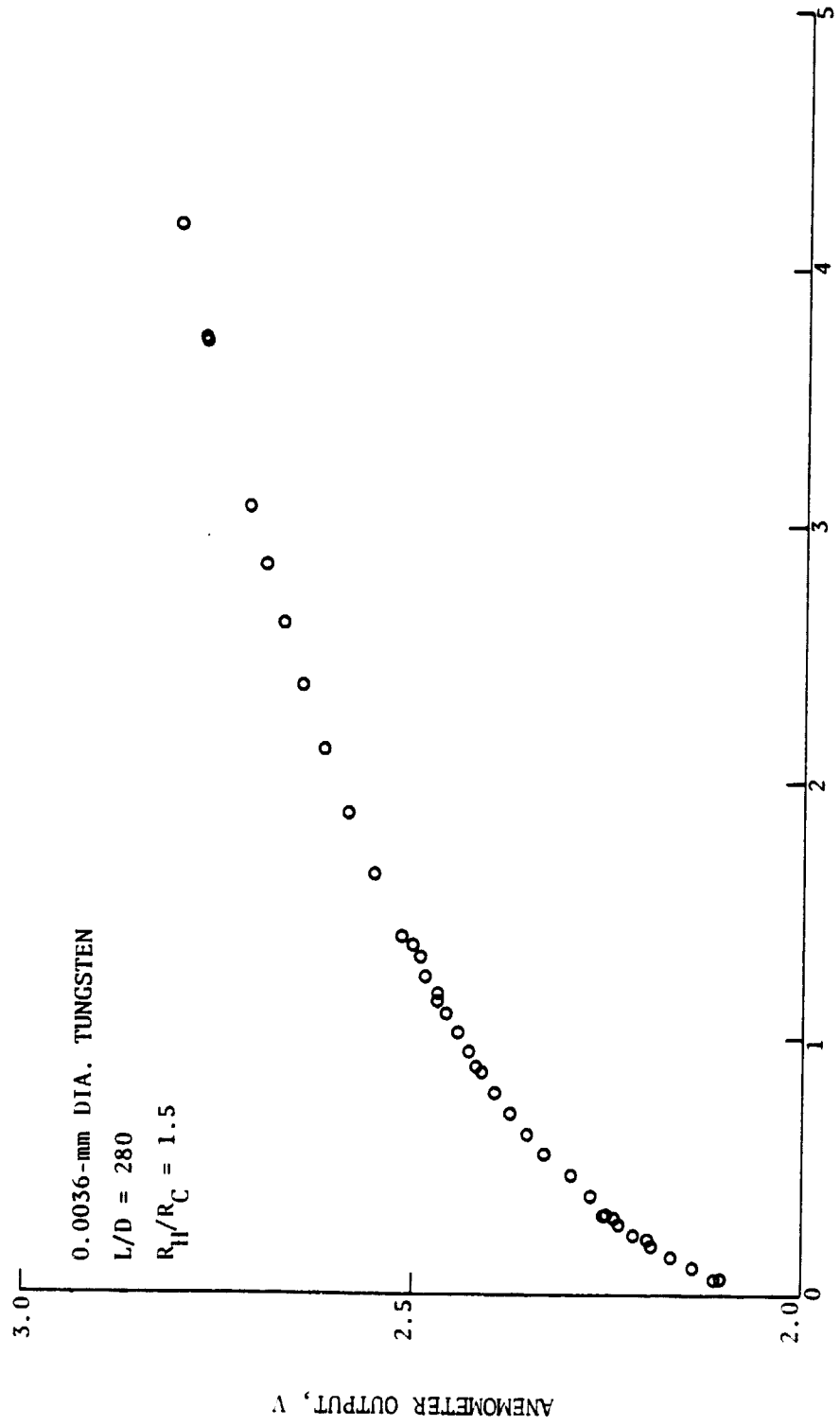

Figure 6. Typical hot wire calibration data.

where E is the anemometer output, U the velocity and A, B and C constants. A representative example of the curve fit using the data from figure 6 is shown in figure 7. Equation (2) was used to reduce the raw boundary-layer velocity profile data. The extension of the above technique to a three-dimensional probe is straightforward.

Flow visualization system.—Flow visualization is provided by Nagib's smoke wire technique (ref. 9). For initial studies, the wire was mounted horizontally 1.3 mm above the splitter plate at X = 304.8 mm. The implementation of the horizontal smoke wire is shown in figure 8. Oil was deposited on the wire by holding a drop to the wire while allowing the weight to pull the wire over the pulley and through the hypodermic tubes. The pull ring anchored the wire in its final position. In operation, the weight and pulley arrangement prevented the wire from sagging when heated by taking up the linear expansion of the wire. Residual oil in the hypodermic tubes blocked any influx of air from disturbing the boundary-layer flow. The tubes also served as points of electrical contact to the wire, which functioned well despite the presence of the oil. This method was found to provide a clear and easily photographable array of streaklines corresponding to the individual droplets formed on the smoke wire.

RESULTS OF PRELIMINARY TEST SECTION SURVEYS

Pressure Gradient

Data obtained for the test section to date include a measurement of the free-stream pressure gradient and mean boundary-layer velocity profiles in the streamwise direction. The streamwise pressure gradient is shown in figure 9. For this data run, the traverse mechanism was not in the test section. As can be seen, aside from the regions of flow acceleration over the leading edge and at the rear of the test section, the maximum pressure change is less than one percent of the free-stream dynamic pressure.

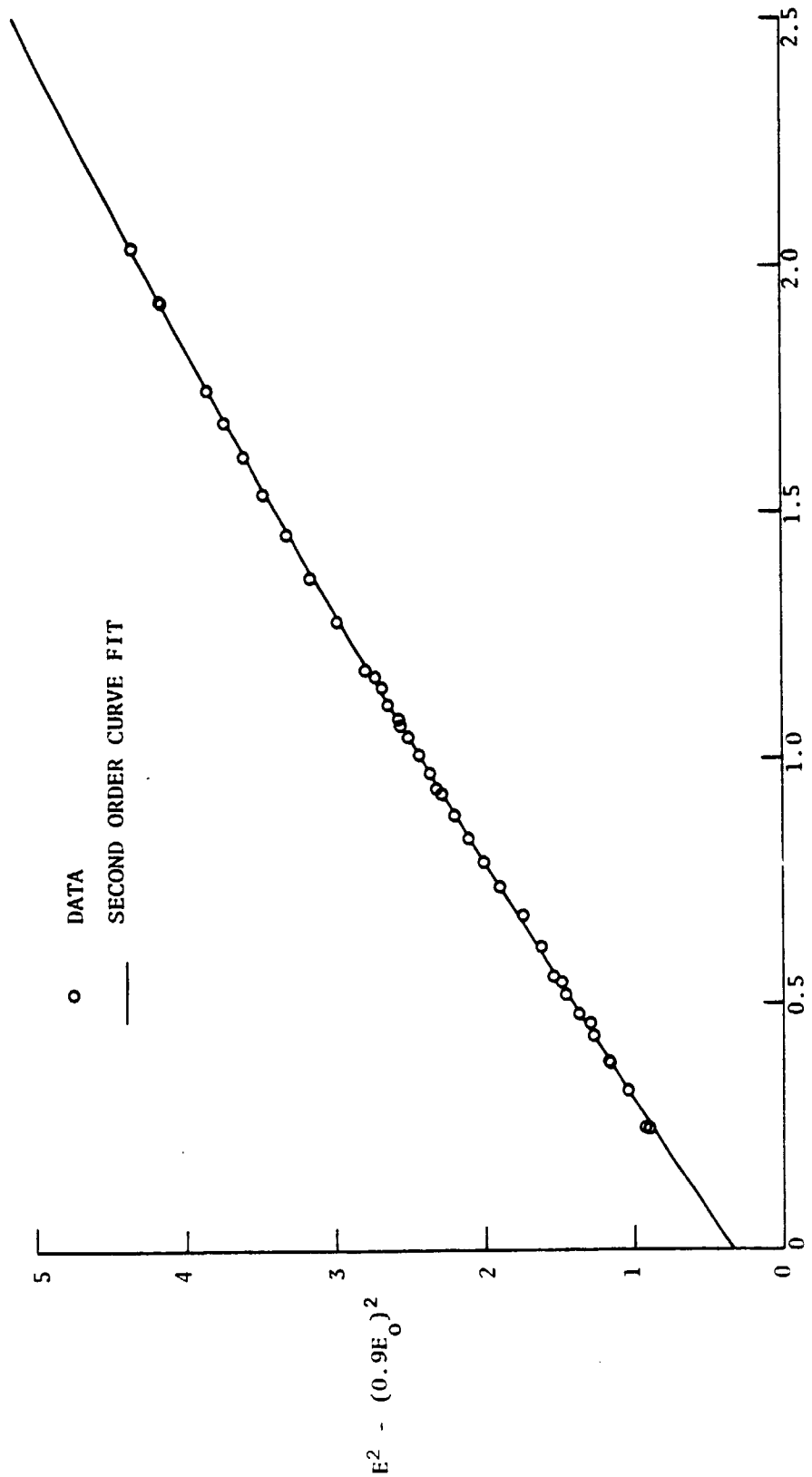

Figure 7. Curve fit of calibration data.

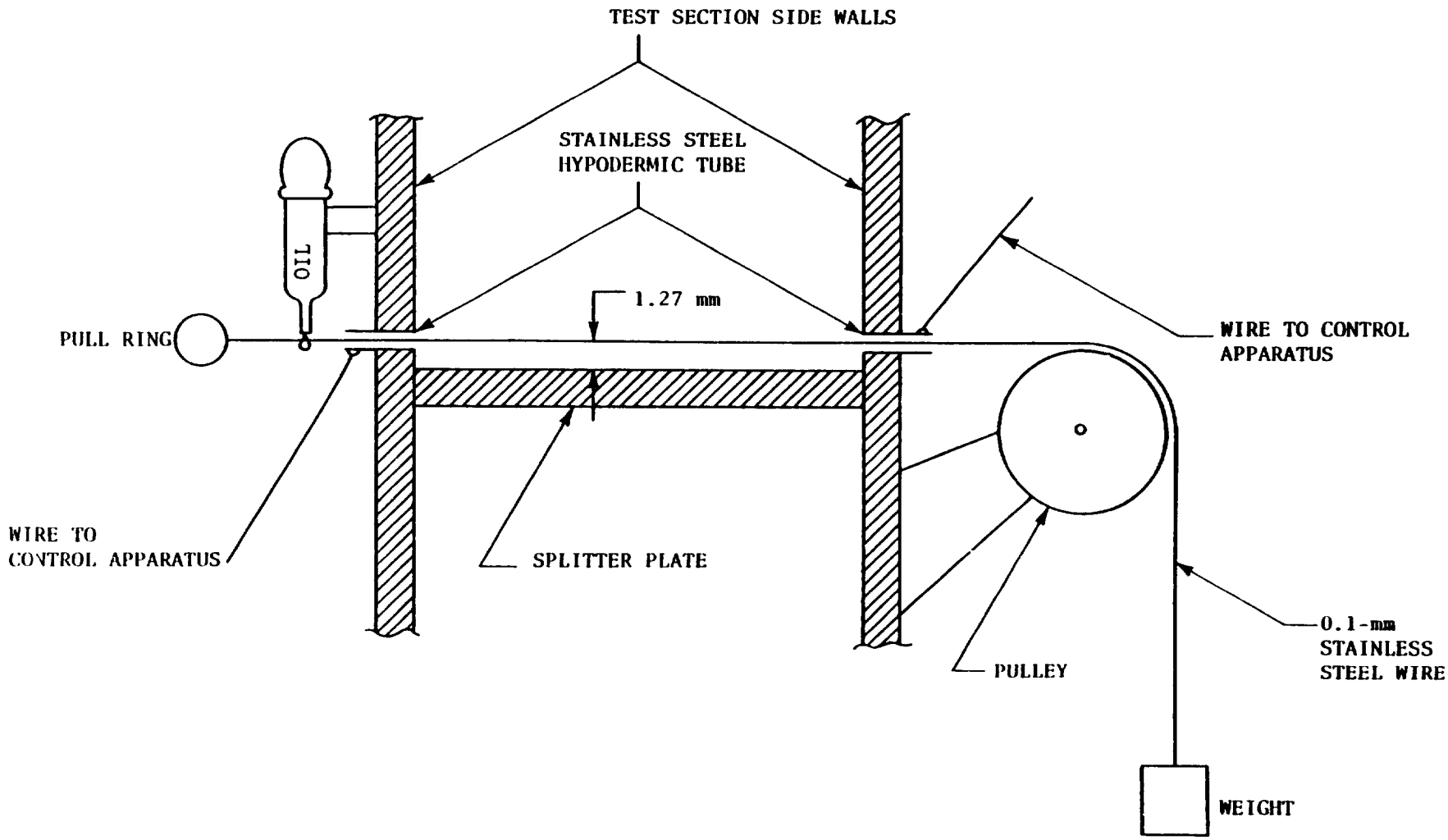

Figure 8. Implementation of horizontal smoke wire.

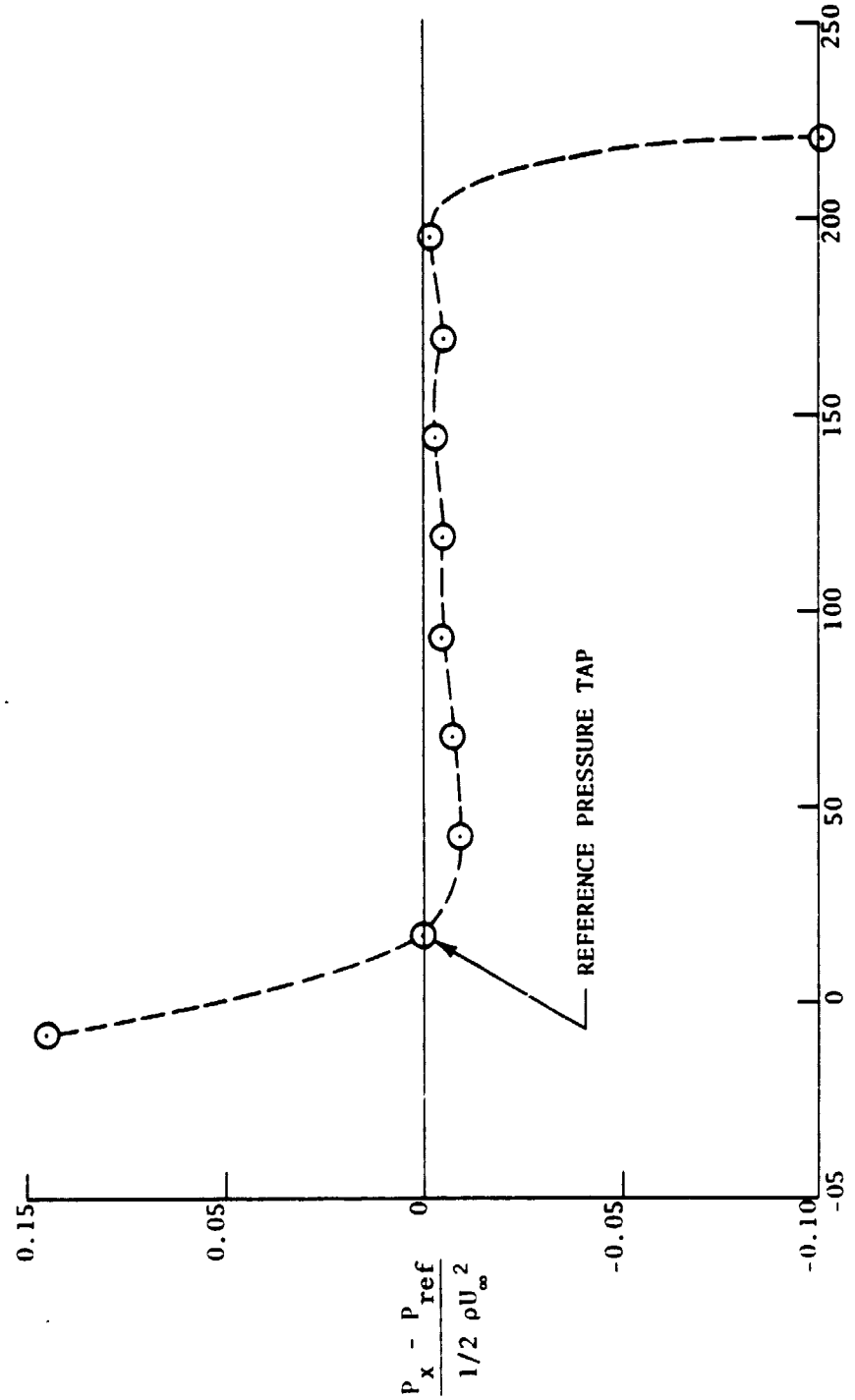

Figure 9. Free-stream static pressure variation.

Mean Velocity Data

A mean velocity boundary-layer profile for X = 852 mm ($Re_x = 1.75 \times 10^5$) is shown in figure 10. As can be seen, the profile is very close to the ideal Blasius profile. The reason for the slight discrepancy can be attributed to the history of the pressure gradient at the leading edge and to experimental accuracy. Figure 11 shows the variation in the shape factor, $H = \delta^*/\theta$, with Re_x. For $Re_x < 10^5$ the profiles are seen to be clearly not fully developed Blasius profiles. This is attributed to the leading edge pressure gradient. After $Re_x = 2 \times 10^5$, the profiles are again seen to deviate from the Blasius with a large scatter. Indications are that the flow was starting to break up, possibly due to leading edge misalignment. Figure 12 shows the growth rate of the boundary layer in terms of Re_θ and Re_x. The data follow the same trend as the Blasius growth rate; however, it would not be expected to be the same due to the effects mentioned above.

REMAINING ITEMS ON EXPERIMENTAL AGENDA

The experiments have been carried through the stages of facility construction and preliminary measurement of boundary-layer mean velocity profiles. Except for construction of the three-dimensional hot wire probe, the assembly of required instrumentation is complete. Remaining items on the experimental agenda are itemized below:

(1) Complete velocity mapping of boundary layer and free stream,

(2) Measurement of free-stream turbulence intensity,

(3) Flow visualization study of isolated hole and partially plugged slot,

(4) Construction of three-dimensional hot wire probe,

(5) Three-dimensional hot wire velocity surveys of isolated hole and plugged slot flow fields, and

(6) Study of correlation between plenum chamber oscillations and flow events in slot/hole or external flow.

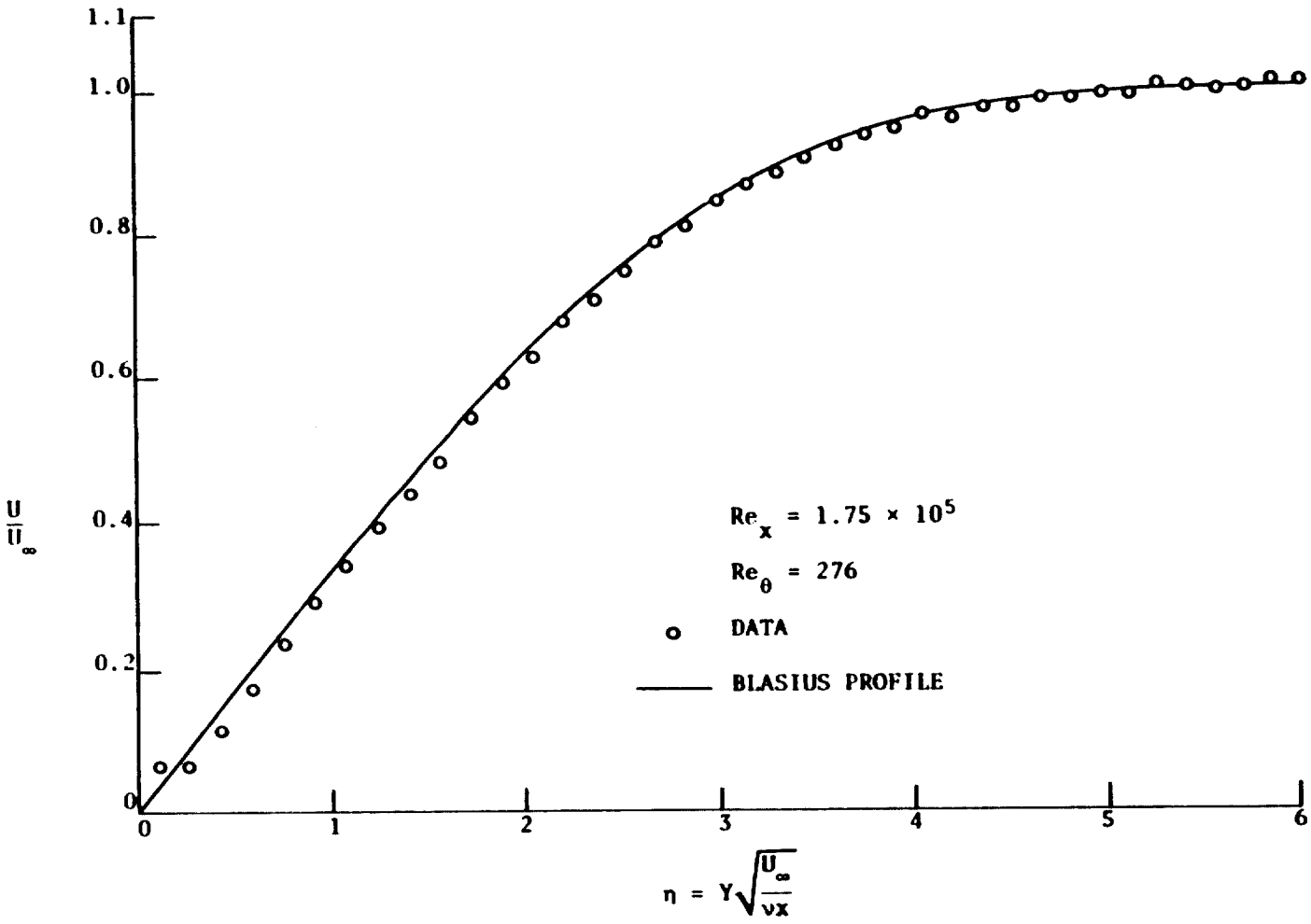

Figure 10. Boundary-layer velocity profile.

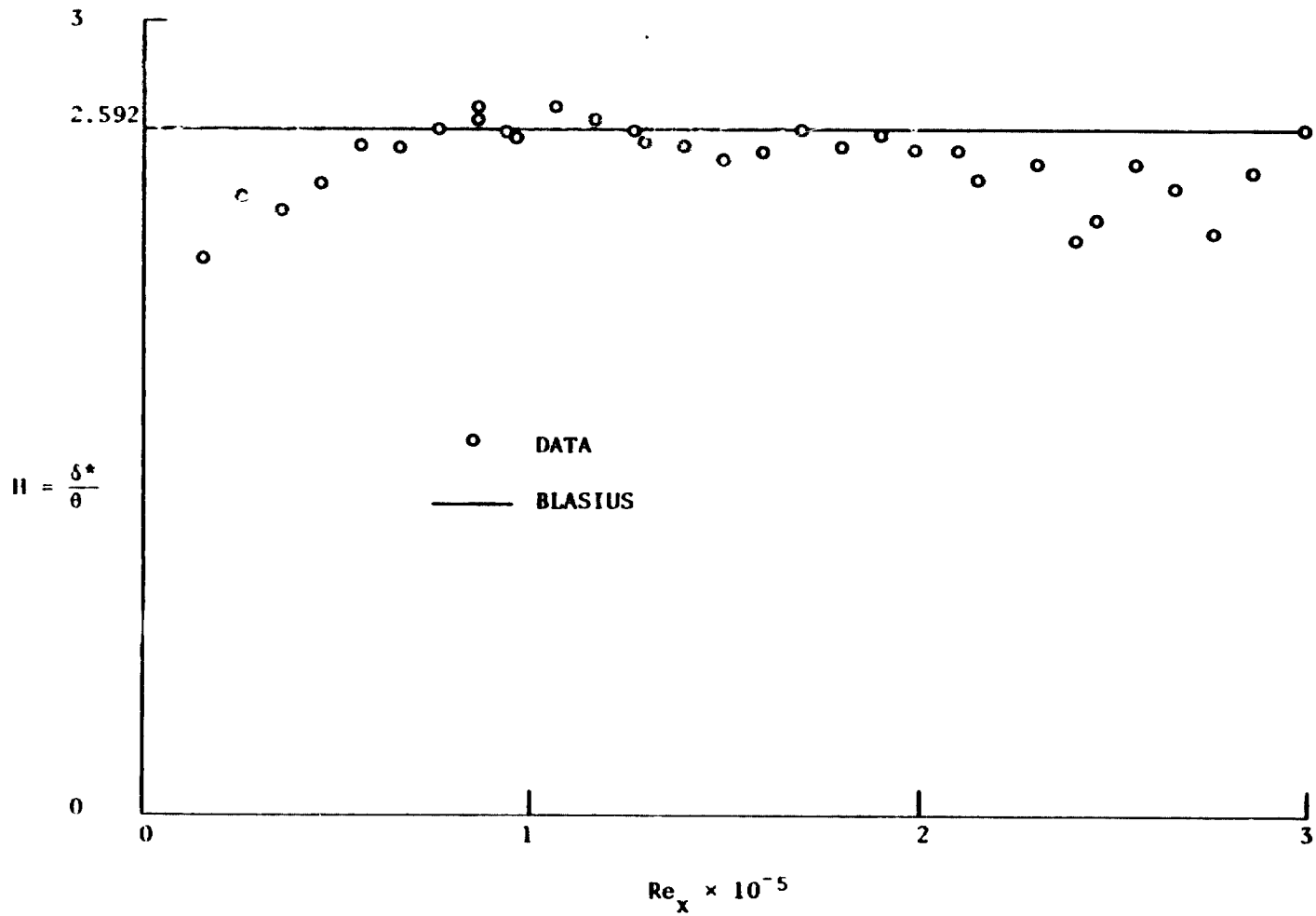

Figure 11. Variation of shape factor with Re_x.

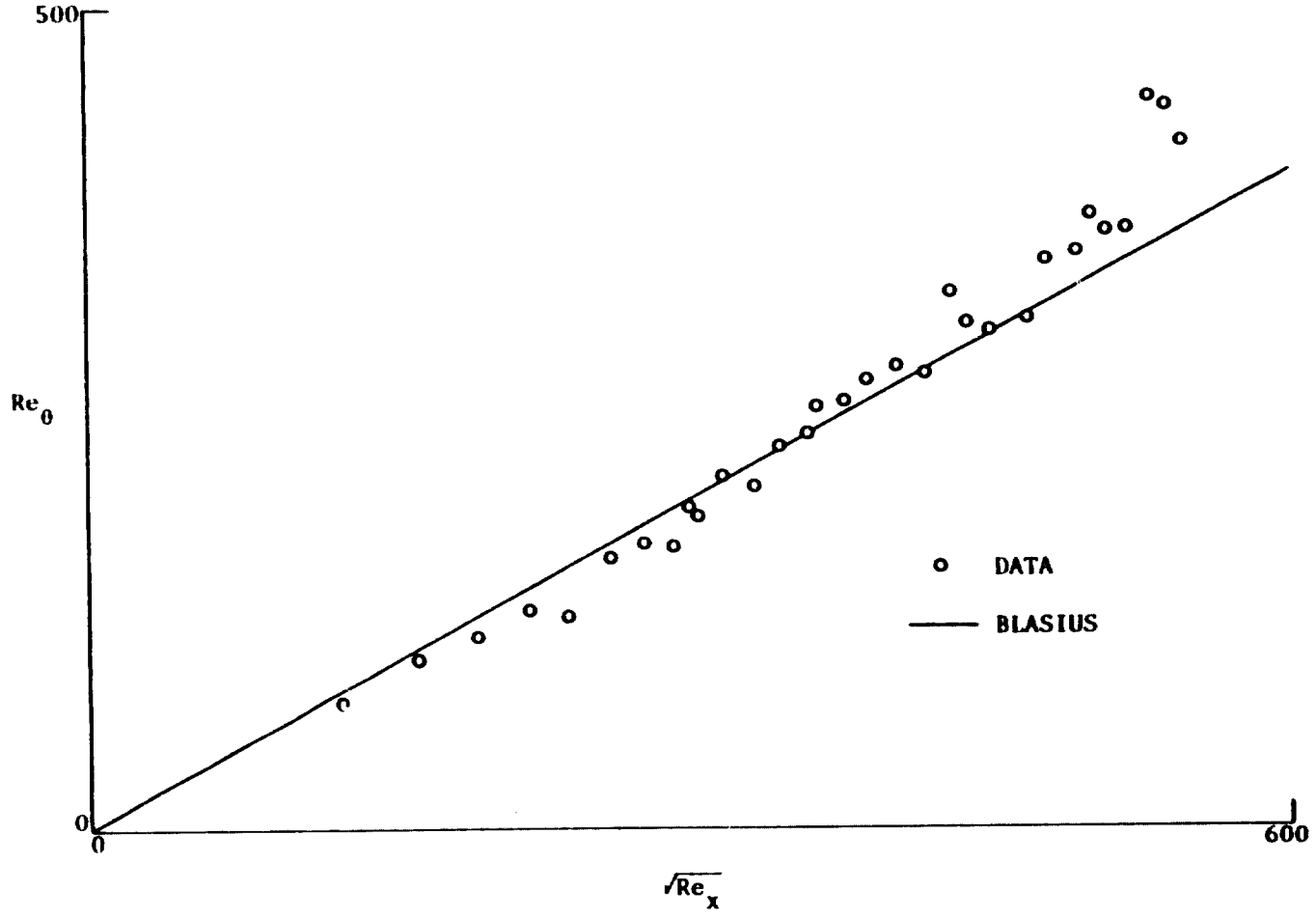

Figure 12. Boundary-layer growth rate.

APPENDIX: ROTATING DISK STABILITY STUDY

Background

The crossflow velocity profile in the three-dimensional boundary layer on a flat rotating disk closely approximates that of a swept wing (ref. 10). The disk presents, therefore, a simple method for study of the crossflow instability, which is of fundamental importance to LFC technology. The first detailed experimental study of the rotating disk was conducted by Gregory, Stuart, and Walker (ref. 11). Using a sublimation flow-visualization technique, they were able to photograph the pattern due to stationary vorticies within the boundary layer. Such stationary vorticies have also been noted on a swept wing (ref. 10). To date no measurements of the three-dimensional transition process for the rotating disk have been made using the hot wire. This is the purpose of the current research. Such data will not only help elucidate the transition process on the disk but will also provide comparison data for the predictions based on linear stability theory (e.g. ref. 12).

Experimental Considerations

The basic consideration for design of an experimental system for study of the crossflow instability on a rotating disk is the transition Reynolds number $\left(\frac{\omega R^2}{\nu}\right)$ which is nominally 300,000 (ref. 11). The rotational speed and diameter of the disk should allow attainment of at least this Reynolds number. In addition, there are other important considerations which are discussed below.

A. Boundary layer thickness.—The hot wire anemometer is the basic tool to be used in studying the boundary-layer disturbances. It is proposed that only the tangential velocity fluctuation be studied initially: Therefore, only a single wire is required, and a thin boundary layer can be accomodated. The expression for the boundary-layer thickness is (ref. 13):

$$\delta = 5\sqrt{\frac{\nu}{\omega}} \qquad (3)$$

B. Signal-to-noise (S/N) ratio.—Disturbances of the ambient air surrounding the disk are analogous to free-stream turbulence in wind-tunnel studies. Therefore, relevant disk velocities should be large compared to ambient air disturbances. This can be accomplished by operating the disk at as high a speed as is consistent with other design considerations. Since the tangential velocity is zero at the center of the disk, it is not possible to maintain a high S/N ratio over all of the disk. It would be preferable if the S/N ratio were large enough at minimum critical Reynolds number to allow accurate determination of that point. Determination of the S/N ratio can only be done experimentally. The minimum critical Reynolds number is $Re_{\delta^*} = 242$ based on calculations by Cebici (ref. 12).

C. Surface roughness.—Surface roughness should not be a variable in the initial studies and, therefore, should be as small as possible. A very general indication of the influence of distributed roughness for no effect on transition is (ref. 13):

$$\frac{U_\infty k_s}{\nu} < 120 \tag{4}$$

For the final disk configuration arrived at, the maximum surface speed is 22.9 m (or 75 ft)/s, corresponding to a maximum permissable roughness height of $k_s = 0.0081$ cm (0.0032 in.). If a polished surface is used, the above criterion is met.

D. Disk vibration.—Unavoidable rotational imbalance of the system will result in fundamental and higher modes of disk vibration. The primary consideration is whether or not such modes couple with stability modes in the boundary layer to produce experimental results which may be unique for a given experimental apparatus. Vibration should, therefore, be kept to a minimum by using appropriate construction techniques (e.g. precision components, resilient mounting of motor, high-vibration impedance coupling of motor to disk, mass loading, etc.). Effects of residual vibration should be checked by cross-correlating the hot wire signal with accelerometer data. Deviation of the disk from true flatness will create an apparent vibration with respect to the stationary hot wire, causing a modulation of the hot wire signal due to the relative

motion of the probe and disk in the steep velocity gradient near the surface. This apparent vibration will also add uncertainty to the position of the probe in the boundary layer. Proper construction technique can minimize deviation from flatness. Axial end play in the rotating system will have a similar effect, however, this can be eliminated entirely by selection of appropriate bearings.

Rotating Disk Apparatus

Based on the above design considerations, a disk system has been designed and constructed with a maximum Reynolds number of 3.39×10^5 and boundary layer thickness of 0.2 cm (0.08 in.). The construction is described below (refer to fig. A1).

The disk is a 48.3-cm (19-in.) diameter, 1.3-cm (0.5-in.) thick piece of Plexiglas which was surface ground to an overall flatness of ±0.00635 mm (±0.00025 in.). The final stage of the grinding process was done with grade 600 silicon carbide grinding compound to attain a near-gloss finish when viewed at a grazing angle. The Plexiglas is attached with screws to a machined 30.5-cm (12-in.) diameter aluminum disk. The drive assembly consists of a 5-cm (2-in.) diameter, 25.4-cm (10-in.) long; drive shaft, mounted in premounted, self-aligning ball bearings; a 2:1 speed-reduction belt drive; and a resiliently mounted 1/4 HP, 1725 rpm syncronous AC motor. The drive assembly is mounted in a rigid steel stand which is mass loaded with several hundred pounds of lead weight. A 30.5-cm diameter aluminum disk identical to the one on the disk assembly is attached to the end of the shaft. The 2 aluminum disks are attached to each other with 12 equally spaced screws around the periphery. By differentially tightening the screws, the disk flexure due to any mounting stresses can be eliminated. By inserting spacer shims between the aluminum disks, the Plexiglas can be aligned to be accurately perpendicular to the drive shaft. Alignment of the system is accomplished by using a dial indicator resolving 0.000254-cm (0.0001-in.) increments on the face of the disk. The entire assembly is housed in a 1.8-m (6-ft) cubical enclosure which serves the dual function of partially isolating the disk from room air movements and of a safety shield in the event of disk breakage. A plywood shield is placed directly behind the disk to isolate the disk from disturbances

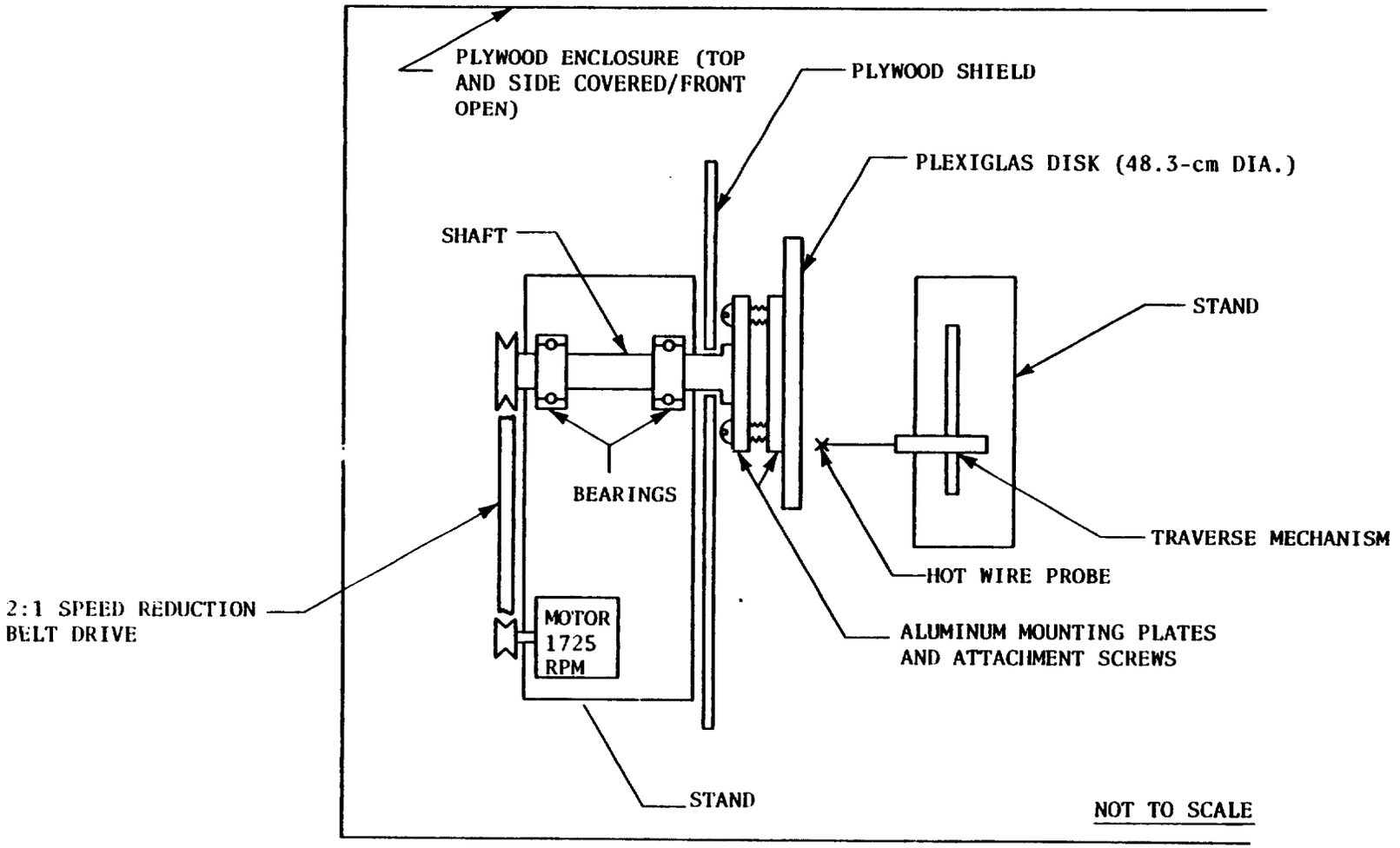

Figure A1. Rotating disk system.

generated by the drive assembly. The hot wire is mounted on a 2-axis traversing mechanism which is mounted on a stand 45.7 cm (18 in.) from the disk.

Instrumentation

The basic piece of instrumentation is a constant temperature, linearized, hot wire anemometer (TSI model 1050 with model 1052 polynomial linearizer). A tungsten wire with an active length of 0.1 cm (0.04 in.) and a diameter of 0.00036 cm (0.00014 in.) is used. The probe is operated perpendicular to the tangential velocity component and parallel to the disk surface. The hot wire is calibrated at approximately room temperature in an open jet.

Other principal items of instrumentation include a Hewlett-Packard (HP) model 3455A digital voltmeter; an HP 3582A digital spectrum analyzer; a Nicolet Explorer III digital oscilloscope; a Kron-Hite 3202R dual high/low pass active filter; and an HP 9825A desk top computer for data acquisition and reduction.

Preliminary Disturbance Growth Rate Data

The design of the system described above was based on experience obtained during several attempts to conduct the disk experiments using standard machine shop equipment (i.e. a grinding disk and a metal turning lathe). For various reasons, these early attempts were not completely successful; however, enough experimental control existed in one case to yield preliminary disturbance growth rate data over a limited Reynolds number range.

That particular experiment utilized a metal turning lathe and allowed a maximum Reynolds number $\left(\frac{\omega R^2}{\nu}\right)$ of 2.13×10^5. The disk was 35.6 cm (14 in.) in diameter and rotated at 1000 rpm. Data was obtained by syncronizing the disk rotation with the sweep rate of an analog oscillocope. Hot wire wave forms corresponding to complete revolutions of the disk were thereby obtained and photographed on the oscilloscope. The mean amplitude of the waveforms was determined from the photographs. Results are plotted in figure A2 and A3. Figure A2 is a plot in linear coordinates

of the relative fluctuation intensity as a function of radius. The plot shows clearly the rapid growth in disturbance amplitude after the stationary vorticies are formed. Figure A3 is the same data plotted in customary growth rate coordinates—the natural logarithm of the relative fluctuation intensity referenced to the intensity at the minimum critical Reynolds number as a function of Reynolds number. This representation tends to expand the ordinate at lower radii. The interesting feature of figure A3 is that, when drawn on a large scale, the curve can be extrapolated to an amplification factor of between e^7 and e^9 at a nominal transition Reynolds number of 3×10^5.

The stationary vorticies numbered 30 or 31 and appeared to be truly stationary with respect to the disk. The number of vorticies is the same as reported in reference 11. There was no indication of higher order traveling waves in the region of the stationary vorticies.

Continuation of Studies

The rotating disk study can be continued using the new apparatus described herein. A tenative test schedule is as follows:

(1). Initial system check concentrating on items such as disk trueness, mechanical vibrations, and ambient air disturbances,

(2). Measurement of broad band amplification rate of tangential component, and

(3). Spectral analysis to determine amplification rate in discrete frequency bands.

An additional item which could be implemented easily is to conduct the same experiments on a disk with concave curvature. This could be accomplished by replacing the flat disk with, for example, a parabolic mirror. This would be of interest since there is currently no experimental growth rate data available for the crossflow instability in regions of concave curvature.

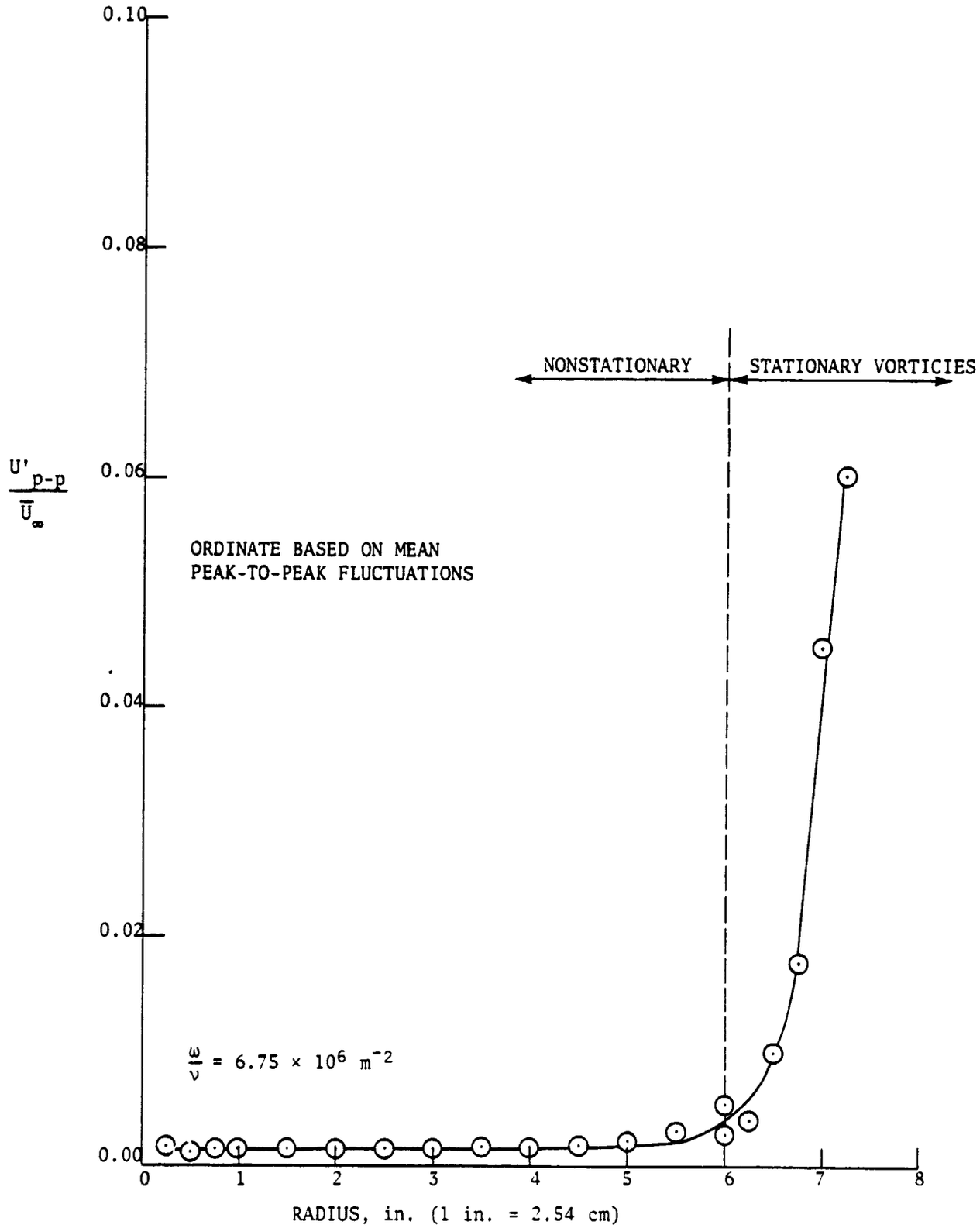

Figure A2. Fluctuation intensity as a function of local radius.

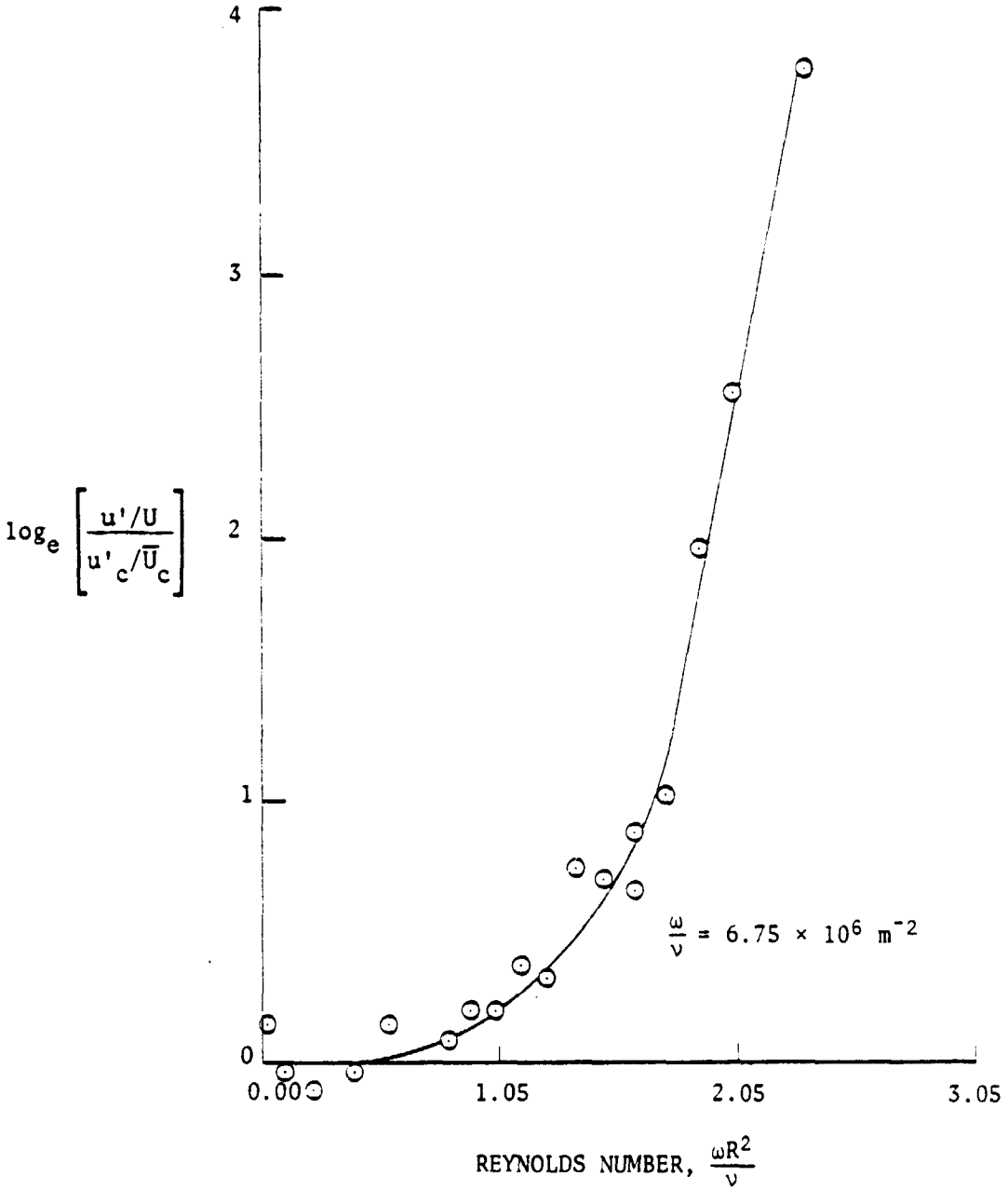

Figure A3. Amplification factor as a function of disk Reynolds number.

REFERENCES

1. Bushnell, D.M.; and Tuttle, M.H.: Survey and Bibliography on Attainment of Laminar Flow Control in Air Using Pressure Gradient and Suction, Volume 1, NASA Reference Publication 1035, Sept. 1979.

2. Gregory, N.: Research on Suction Surfaces for Laminar Flow. Boundary Layer and Flow Control, Volume 2, G.V. Lachman, ed., Pergamon Press, 1961, pp. 924-960.

3. Goldsmith, J.: Critical Laminar Suction Parameters for Suction into an Isolated or a Single Row of Holes, Northrop Report NAI-57-529, Feb. 1957.

4. Goldsmith, J.: Experiments with Laminar Boundary Layer Suction Through Rows of Closely Spaced Circular Holes at High Reynolds Number and Low Turbulence. Rep. No. BLC-36, Northrop Aircraft, Inc., Mar. 1954.

5. Pfenniger, W.: Laminar Flow Control, Laminarization. Special Course on Concepts for Drag Reduction. AGARD Report No. 654, 1977, pp. 3-1 to 3-75.

6. Evaluation of Laminar Flow Control System Concepts for Subsonic Commerical Transport Aircraft. NASA CR-158976, Dec. 1978.

7. Pfenniger, W.; Bacon, J.; and Goldsmith, J.: Flow Disturbances Induced by Low Drag Boundary Layer Suction Through Slots. Phys. Fluids Suppl., Vol. 10, No. 9, Pt. 2, Sept. 1967, pp. S112-S114.

8. Holt, C.F.: The Laminar Boundary Layer in the Vicinity of a Suction Slot. M.S. Thesis, Pennsylvania State Univ., 1965.

9. Corke, T.; Koga, D.; Drubka, R.; and Nagib, H.: A New Technique for Introducing Controlled Sheets of Smoke Streaklines in Wind Tunnels. ICIASF '77 RECORD (New York), 1977, pp. 74-80.

10. Poll, D.I.A.: Some Aspects of the Flow Near a Swept Attachment Line with Particular Reference to Boundary Layer Transition. C of A Report 7805, Cranfield College of Aeronautics, Aug. 1978.

11. Gregory, N.; Stuart, J.T.; and Walker, W.S.: On the Stability of Three-Dimensional Boundary Layers with Application to the Flows due to a Rotating Disk. Philos. Trans. R. Soc. London, No. 943, Vol. 248, pp. 155-199, July 14, 1955.

12. Cebeci, T; and Keller, H.B.: Stability Calculations for a Rotating Disk. Laminar-Turbulent Transition, AGARD Conference Proceedings No. 224, May 1977.

13. Schlichting, H.: Boundary Layer Theory, 6th Edition, McGraw-Hill, 1968.